

Gesture-Aware Indoor THz ISAC Systems for Adaptive Resource Allocation

Zhonghao Liu*, Yinchao Yang*, Yahao Ding*, Yixuan Wang*, and Mohammad Shikh-Bahaei*

*King's College London

Email: {zhonghao.liu, yinchao.yang, yahao.ding, k21040372, m.sbahaei}@kcl.ac.uk

Abstract—This paper investigates a multi-user indoor integrated sensing and communication (ISAC) system operating in the terahertz (THz) band, designed for adaptive communication based on gesture recognition. Leveraging gesture tracking through an extended Kalman filter (EKF), the access point (AP) dynamically adjusts resource allocation in response to detected gesture variations, thereby improving sensing accuracy. Based on the gesture recognition results, the AP further updates the communication quality requirements of different users, enabling efficient resource allocation. To this end, an adaptive joint optimization algorithm for power allocation and beamforming is developed to maximize the overall sensing signal-to-interference-plus-noise ratio (SINR) while satisfying the gesture-dependent communication quality of service (QoS) constraints. Simulation results demonstrate that the proposed method effectively responds to gesture dynamics, achieving superior sensing accuracy and communication performance compared with conventional single-variable optimization baselines.

Index Terms—ISAC, gesture recognition, THz, indoor communication.

I. INTRODUCTION

As 6G approaches, wireless networks are evolving from conventional data transmission platforms into intelligent systems capable of environmental sensing, autonomous decision-making, and adaptive control. Integrated sensing and communication (ISAC), a key enabler of this paradigm shift, aims to jointly perform communication and sensing functions within a unified system architecture and shared spectral resources, thereby enhancing spectral efficiency and reducing system overhead. ISAC technology is paving the way for a wide range of intelligent applications, including autonomous driving, smart homes, and human machine interaction [1]. In immersive XR/VR and smart indoor spaces, human gestures act as a natural control interface and often coincide with abrupt changes in traffic demand and latency constraints, which calls for sensing-assisted and context-aware resource adaptation. The terahertz (THz) band provides an attractive platform for ISAC systems because its short wavelength enables high resolution sensing, and its wide bandwidth supports high data rates [2]. Consequently, THz-based ISAC is particularly well-suited to compact and dynamic indoor environments, such as gesture recognition scenarios.

In indoor environments, communication requirements are highly dynamic, as user demands vary with their behavioral state. For example, picking up a smart device typically indicates an active interaction session (e.g., video call, messaging, XR control), whereas putting it down often corresponds

to an idle state. As a result, the QoS constraints may change abruptly over time, making static designs ineffective. Consequently, intelligent and adaptive resource allocation is required to track user behavior and jointly accommodate time-varying communication demands and sensing tasks.

In previous studies, extensive research efforts have been devoted to THz and ISAC systems. For instance, Li *et al.* [3] leveraged sensing data to predict user trajectories and velocities, thereby enabling timely beam adjustments and mitigating communication blockages. Fang *et al.* [4] demonstrated fine-grained environmental reconstruction and material identification, verifying the high resolution and feasibility of THz sensing in complex indoor environments. Zhou *et al.* [5] enhanced sensing accuracy through optimized beamforming and transmission design, while maintaining communication quality. Furthermore, adaptive communication techniques for dynamic environments have also been explored. For example, Bacchielli *et al.* [6] proposed a THz MIMO-OFDM ISAC framework for cluttered indoor environments, enabling target tracking and other sensing functions while sustaining high data rates. However, most existing works primarily focus on static scenarios and overlook the dynamic variations in user gestures and behaviors, as well as their impact on real-time resource optimization in THz-ISAC indoor systems.

Inspired by these works, we propose a sensing-assisted THz ISAC system that dynamically infers the user's communication requirements based on the recognized gesture results, enabling more efficient resource allocation between sensing and communication. The system continuously monitors hand gestures (e.g., picking up or putting down a device) to infer the user activity state and adjust the QoS accordingly. When active usage is detected, more power is allocated to communication; otherwise, communication power is reduced to suppress interference and improve sensing performance.

The main contributions of this work are summarized as follows:

- We investigate an indoor THz-ISAC system under dynamic user scenarios, where gesture variations lead to time-varying communication and sensing demands.
- We construct a mapping mechanism from gesture states to communication QoS requirements, through which the user's communication QoS demand can be inferred from the recognized gesture state.
- We design a tracking module based on echo signal processing that predicts gesture transitions and provides

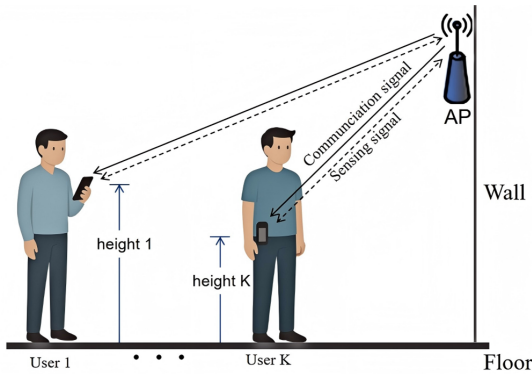


Figure 1: The indoor THz-ISAC system, where an access point is deployed at the corner of the room and transmits both communication and sensing signals.

real-time state estimation for adaptive resource management.

II. SYSTEM MODEL

As shown in Fig. 1, we consider a THz-ISAC system, where an access point (AP) simultaneously serves K single-antenna users and performs gesture sensing. The AP is equipped with a uniform linear array (ULA) consisting of M antennas. Specifically, hand gestures such as picking up or putting down a device are modeled as changes in the vertical position of the user's hand. For simplicity, the device height is assumed to be h_A after picking up and h_B after putting down.

A. Signal Model

At time slot l , the AP transmits a dual-functional signal to support both communication and sensing, which can be expressed as:

$$\mathbf{x}[l] = \mathbf{W}_c \mathbf{s}_c[l] + \mathbf{W}_r \mathbf{s}_r[l], \quad (1)$$

where $\mathbf{W}_c = [\sqrt{P_1} \mathbf{w}_{c,1}, \dots, \sqrt{P_K} \mathbf{w}_{c,K}] \in \mathbb{C}^{M \times K}$ denotes the communication beamforming matrix, and $\mathbf{W}_r = \sqrt{P_r} [\mathbf{w}_{r,1}, \dots, \mathbf{w}_{r,K}] \in \mathbb{C}^{M \times K}$ denotes the sensing beamforming matrix. Here, P_k denotes the transmit power allocated to the user k and the sensing power P_r is uniformly applied across all sensing beams. Each user k is associated with a communication beamforming vector $\mathbf{w}_{c,k} \in \mathbb{C}^{M \times 1}$ and a sensing beamforming vector $\mathbf{w}_{r,k} \in \mathbb{C}^{M \times 1}$. The communication symbols for the K users at time slot l are denoted by $\mathbf{s}_c[l] \in \mathbb{C}^K$, which consists of mutually orthogonal symbols across different users, such that $\mathbb{E}[\mathbf{s}_c[l] \mathbf{s}_c^H[l]] = \mathbf{I}_K$. Similarly, the radar signal vector contains K orthogonal waveforms for K users, denoted by $\mathbf{s}_r[l] \in \mathbb{C}^K$, satisfying $\mathbb{E}[\mathbf{s}_r[l] \mathbf{s}_r^H[l]] = \mathbf{I}_K$. Furthermore, communication symbols and radar waveforms are assumed to be statistically independent, satisfying $\mathbb{E}[\mathbf{s}_c[l] \mathbf{s}_r^H[l]] = 0$.

In the proposed ISAC system, the AP transmits the dual-functional signal to the users. Therefore, the received signal by user k at time slot l is given by [7]:

$$\begin{aligned} y_k[l] = & \mathbf{h}_k^H \sqrt{P_k} \mathbf{w}_{c,k} s_{c,k}[l] + \sum_{j \neq k} \mathbf{h}_k^H \sqrt{P_j} \mathbf{w}_{c,j} s_{c,j}[l] \\ & + \mathbf{h}_k^H \sqrt{P_r} \mathbf{w}_{r,k} s_{r,k}[l] + n_k[l], \end{aligned} \quad (2)$$

where $\mathbf{h}_k \in \mathbb{C}^{M \times 1}$ is the wireless channel vector of the user k , the detailed modeling of \mathbf{h}_k will be introduced in the next subsection, and $n_k[l] \sim \mathcal{CN}(0, \sigma_n^2)$ is the Gaussian noise. The received echo signal can be expressed as:

$$\mathbf{y}_{\text{echo}}[l] = \sum_{k=1}^K \mathbf{G}_k^H \mathbf{x}[l - \tau_k] + \mathbf{n}_r[l], \quad (3)$$

where $\mathbf{G}_k \in \mathbb{C}^{M \times M}$ is the channel matrix of user k , and its formulation will be discussed in the next subsection. In addition, τ_k denotes the propagation delay of the echo signal and $\mathbf{n}_r[l] \sim \mathcal{CN}(0, \sigma_r^2)$ is the Gaussian noise.

B. Channel Model

Due to the significant path loss and inherent sparsity of THz waveforms [8], we focus solely on the line-of-sight (LoS) channel. The channel between the AP and user k is given by:

$$\mathbf{h}_k = \frac{c}{4\pi f d_k} e^{-\frac{1}{2} K(f) d_k} \mathbf{a}(\theta_k), \quad (4)$$

where the term $\frac{c}{4\pi f d_k} e^{-\frac{1}{2} K(f) d_k}$ represents the THz path loss. Here, c is the speed of light, f is the carrier frequency, d_k is the distance between the AP and user k , and $K(f)$ is the molecular absorption coefficient at frequency f , which can be obtained from HITRAN database [9]. The term $\mathbf{a}(\theta_k)$ denotes the array response vector at the AP for the departure angle θ_k , given as $\mathbf{a}(\theta_k) = [1, e^{j \frac{2\pi d}{\lambda} \sin \theta_k}, \dots, e^{j \frac{2\pi (M-1)d}{\lambda} \sin \theta_k}]^T$.

Similarly, the target's reflection channel can be modeled as:

$$\mathbf{G}_k = \left(\frac{c}{4\pi f d_k} \right)^2 e^{-K(f) d_k} \beta_k e^{-j \frac{4\pi f v_k t}{c}} \mathbf{a}(\theta_k) \mathbf{a}^H(\theta_k), \quad (5)$$

where β_k is the radar cross-section (RCS) of the user k .

C. Performance Measurement

We adopt signal-to-interference-plus-noise ratio (SINR) as the performance metric for both communication and sensing. The communication SINR of user k at time slot l is expressed as:

$$\begin{aligned} \text{SINR}_{\text{com},l}^k = & \frac{P_{k,l} |\mathbf{h}_{k,l}^H \mathbf{w}_{c,k,l}|^2}{\sum_{j=1, j \neq k}^K P_{j,l} |\mathbf{h}_{k,l}^H \mathbf{w}_{c,j,l}|^2 + P_{r,l} \sum_{j=1}^K |\mathbf{h}_{k,l}^H \mathbf{w}_{r,j,l}|^2 + \sigma_n^2}, \end{aligned} \quad (6)$$

where the subscript l indexes the time slot l .

When the user picks up the device, for example, to send a message, it indicates a higher communication demand, and thus a higher communication SINR is required, denoted by $\text{SINR}_{\text{com}}^{\text{high}}$. Conversely, when the user puts down the device, the communication demand is reduced, and a lower SINR

requirement $\text{SINR}_{\text{com}}^{\text{low}}$ is applied. We define the required communication SINR threshold of user k as a function of gesture state, expressed as:

$$\gamma_{k,l}^{\text{req}} = \delta_{k,l} \text{SINR}_{\text{com}}^{\text{high}} + (1 - \delta_{k,l}) \text{SINR}_{\text{com}}^{\text{low}}, \quad (7)$$

where $\delta_{k,l} \in \{0,1\}$ is a binary indicator representing the communication requirement of user k at time slot l , which is dependent on the gesture. When the user is recognized as picking up the device, we set $\delta_{k,l} = 1$ to impose a higher communication requirement; otherwise, we set $\delta_{k,l} = 0$.

In the modeling of the reflected sensing signals, we assume that the number of antennas at the AP satisfies $M \gg K$. Under this condition, the reflected signals from different users exhibit strong spatial separability, and the mutual interference between users becomes negligible [10]. Therefore, the sensing SINR is given by:

$$\text{SINR}_{\text{sen},l}^k = \frac{P_{r,l} |\mathbf{G}_{k,l} \mathbf{w}_{r,k,l}|^2}{P_{k,l} |\mathbf{G}_{k,l} \mathbf{w}_{c,k,l}|^2 + \sigma_r^2}. \quad (8)$$

III. GESTURE MOVEMENT MODEL AND STATE PREDICTION

A. Gesture state movement model

The gesture motion is modeled as a discrete-time state-space system under the assumption of constant velocity within each time slot l . Using a matched filter, the time delay $\tau_{l,k}$ and the Doppler shift f_l can be estimated. Based on that, the distance between the antenna and the hand of the user k can be expressed as $d_{l,k} = \frac{c \cdot \tau_{l,k}}{2}$ with c being the speed of light.

The constant speed $v_{l,k}$ can be decomposed into a radial component $v_{l,k}^r$ and a tangential component $v_{l,k}^t$ at the time slot l , with respect to the line connecting the hand and the antenna. We assume that $\theta_{l,k}$ denotes the angle of arrival (AoA) of user k at time slot l . The radial and tangential velocities $v_{l,k}^r$ and $v_{l,k}^t$ are treated as known inputs which can be obtained following the model in [11]. Therefore, the distance and AoA for user k at the next time slot are given by:

$$d_{l,k} = d_{l-1,k} - v_{l-1,k}^r T, \quad \theta_{l,k} = \theta_{l-1,k} + \frac{v_{l-1,k}^t T}{d_{l-1,k}}, \quad (9)$$

where T is the length of the time slot.

We observe that the device height typically increases when the users pick up the device and decreases when the device is put down. Therefore, we use the variation in device height as the primary feature for gesture recognition. Specifically, the height change is defined as $\Delta h_{l,k} = h_{l,k} - h_{l-1,k}$, where the device height at time slot l is calculated by $h_{l,k} = d_{l,k} \cos \theta_{l,k}$. Therefore, based on the echo information obtained at time slot l and the predicted distance and angle at time slot $l+1$, we compute the height variation to determine whether a gesture has occurred. To determine whether a gesture actually occurs (as opposed to small fluctuations or

noise), we introduce a height variation threshold ϵ_h . Therefore, the decision rule for gesture state change is defined as:

$$\begin{cases} \text{inactive,} & |\Delta h_{l,k}| < \epsilon_h, \\ \text{picking up,} & |\Delta h_{l,k}| \geq \epsilon_h \text{ and } \Delta h_{l,k} > 0, \\ \text{putting down,} & |\Delta h_{l,k}| \geq \epsilon_h \text{ and } \Delta h_{l,k} < 0. \end{cases} \quad (10)$$

Once the system recognizes that user k is picking up the device, the communication SINR is immediately raised to $\text{SINR}_{\text{com}}^{\text{high}}$, $\delta_{k,l}$ is set to 1. Conversely, when the device is put down, $\delta_{k,l}$ is set to 0. If the gesture state is inactive, $\delta_{k,l}$ retains its previous value.

B. Extended Kalman Filtering

In this part, we propose an extended Kalman filter (EKF) for gesture state prediction and tracking. In the system with K users, the state of the user k at time slot $l-1$ is defined by the distance and the AoA relative to the AP, and the state vector is denoted as $\mathbf{x}_{l-1,k} = [d_{l-1,k}, \theta_{l-1,k}]^T$. The measured vector at time slot l is denoted as $\mathbf{z}_{l,k} = [\tau_{l,k}, \theta_{l,k}]^T$. Thus, the model can be recast in compact forms as:

$$\begin{cases} \text{State Evolution Model:} & \mathbf{x}_{l,k} = \mathbf{f}(\mathbf{x}_{l-1,k}) + \mathbf{Q}_{l,k}, \\ \text{Measurement Model:} & \mathbf{z}_{l,k} = \mathbf{h}(\mathbf{x}_{l,k}) + \mathbf{R}_{l,k}, \end{cases} \quad (11)$$

where $\mathbf{f}(\cdot)$ is defined in (9), and $\mathbf{Q}_{l,k} = [Q_{\theta,k}, Q_{d,k}]^T$ denotes the process noise vector, which is independent of $\mathbf{f}(\mathbf{x}_{l-1,k})$. According to \mathbf{y}_{echo} in (3), we can obtain measurement model for user k . Similarly, the measurement noise $\mathbf{R}_{l,k} = [R_{\tau,k}, R_{\theta,k}]^T$ is independent of $\mathbf{h}(\mathbf{x}_{l-1,k})$. As considered above, both $\mathbf{Q}_{l,k}$ and $\mathbf{R}_{l,k}$ follow zero-mean Gaussian distributions, with covariance matrices being expressed as:

$$\mathbf{Q}_s = \text{diag}(\sigma_d^2, \sigma_{\theta}^2), \mathbf{R}_m = \text{diag}(\sigma_{\tau}^2, \sigma_{\theta}^2). \quad (12)$$

In order to linearize the models, the Jacobian matrices for both $\mathbf{f}(\mathbf{x}_{l,k})$ and $\mathbf{h}(\mathbf{x}_{l,k})$ need to be computed. By straightforward differentiation, the Jacobian of $\mathbf{f}(\mathbf{x}_{l-1,k})$ is given as:

$$\left. \frac{\partial \mathbf{f}}{\partial \mathbf{x}} \right|_{\mathbf{x}=\hat{\mathbf{x}}_{l-1,k}} = \begin{bmatrix} 1 & 0 \\ -\frac{v_{l-1,k}^t T}{(d_{l-1,k})^2} & 1 \end{bmatrix}. \quad (13)$$

The Jacobian of $\mathbf{h}(\mathbf{x}_{l,k})$ is:

$$\left. \frac{\partial \mathbf{h}}{\partial \mathbf{x}} \right|_{\mathbf{x}=\hat{\mathbf{x}}_{l,k}} = \begin{bmatrix} \frac{2}{c} & 0 \\ 0 & 1 \end{bmatrix}. \quad (14)$$

Based on (13) and (14), following the standard procedure of Kalman filtering [12], the gesture state prediction and tracking design is summarized as follows:

1) State Prediction:

$$\hat{\mathbf{x}}_{l,k|l-1,k} = \mathbf{f}(\hat{\mathbf{x}}_{l-1,k}). \quad (15)$$

2) Linearization:

$$\mathbf{F}_{l-1,k} = \left. \frac{\partial \mathbf{f}}{\partial \mathbf{x}} \right|_{\mathbf{x}=\hat{\mathbf{x}}_{l-1,k}}, \mathbf{H}_{l,k} = \left. \frac{\partial \mathbf{h}}{\partial \mathbf{x}} \right|_{\mathbf{x}=\hat{\mathbf{x}}_{l,k|l-1,k}}. \quad (16)$$

3) MSE Matrix Prediction:

$$\mathbf{M}_{l,k|l-1,k} = \mathbf{F}_{l-1,k} \mathbf{M}_{l-1,k} \mathbf{F}_{l-1,k}^H + \mathbf{Q}_s. \quad (17)$$

4) Kalman Gain Calculation:

$$\mathbf{G}_{l,k} = \mathbf{M}_{l,k|l-1,k} \mathbf{H}_{l,k}^H (\mathbf{R}_m + \mathbf{H}_{l,k} \mathbf{M}_{l,k|l-1,k} \mathbf{H}_{l,k}^H)^{-1}. \quad (18)$$

5) State Tracking:

$$\hat{\mathbf{x}}_{l,k} = \hat{\mathbf{x}}_{l,k|l-1,k} + \mathbf{G}_{l,k} (\mathbf{z}_{l,k} - \mathbf{h}(\hat{\mathbf{x}}_{l,k|l-1,k})). \quad (19)$$

6) MSE Matrix Update:

$$\mathbf{M}_{l,k} = (\mathbf{I} - \mathbf{G}_{l,k} \mathbf{H}_{l,k}) \mathbf{M}_{l,k|l-1,k}. \quad (20)$$

IV. PROBLEM FORMULATION

During time slot l , we aim to jointly optimize the beamforming vector and power to maximize the sum sensing SINR while ensuring the power constraints and communication SINR requirements. We denote the optimization variables at time slot l as $P_{r,l}$, $P_{k,l}$, $\mathbf{w}_{c,k,l}$, $\mathbf{w}_{r,k,l}$, and the sensing channel as $\mathbf{G}_{k,l}$. The optimization problem shown as:

$$\max_{P_{k,l}, P_{r,l}, \mathbf{w}_{c,k,l}, \mathbf{w}_{r,k,l}} \sum_{k=1}^K \frac{P_{r,l} |\mathbf{G}_{k,l} \mathbf{w}_{r,k,l}|^2}{P_{k,l} |\mathbf{G}_{k,l} \mathbf{w}_{c,k,l}|^2 + \sigma_r^2} \quad (21a)$$

$$\text{s.t.} \quad KP_{r,l} + \sum_{k=1}^K P_{k,l} \leq P_{\max}, \quad (21b)$$

$$P_{r,l} \geq 0, \quad P_{k,l} \geq 0, \quad \forall k, \quad (21c)$$

$$\|\mathbf{w}_{c,k,l}\|^2 = 1, \quad \forall k, \quad (21d)$$

$$\|\mathbf{w}_{r,k,l}\|^2 = 1, \quad \forall k, \quad (21e)$$

$$\text{SINR}_{\text{com},l}^k \geq \gamma_{k,l}^{\text{req}}, \quad \forall k, \quad (21f)$$

where P_{\max} is the total power constraint and (21b) imposes the total transmit-power budget. Constraints (21d) and (21e) enforce unit-norm constraints on the communication and sensing beamforming vectors $\|\mathbf{w}_{c,k,l}\|$ and $\|\mathbf{w}_{r,k,l}\|$, respectively. However, the presence of fractional terms in both the objective function (21a) and the constraints renders the problem non-convex and challenging to solve directly. To address these challenges, we propose utilizing the fractional programming (FP) and alternating optimization (AO) methods to reformulate problem (21) into a tractable convex optimization problem, which is then solved iteratively. Since (21a) is in the form of a sum of fractional ratios, we apply the quadratic transform and introduce an auxiliary variable $\mathbf{t}_1 = [t_{1,l}, t_{2,l}, \dots, t_{K,l}]^T$, which reformulates it as follows:

$$(21a) \rightarrow \sum_{k=1}^K 2t_{k,l} \sqrt{P_{r,l} |\mathbf{G}_{k,l} \mathbf{w}_{r,k,l}|^2} - \sum_{k=1}^K t_{k,l}^2 \left(P_{k,l} |\mathbf{G}_{k,l} \mathbf{w}_{c,k,l}|^2 + \sigma_r^2 \right). \quad (22)$$

Given other variables, the optimal solution for the auxiliary variable $t_{k,l}$ can be expressed as follows:

$$t_{k,l} = \frac{\sqrt{P_{r,l} |\mathbf{G}_{k,l} \mathbf{w}_{r,k,l}|^2}}{P_{k,l} |\mathbf{G}_{k,l} \mathbf{w}_{c,k,l}|^2 + \sigma_r^2}. \quad (23)$$

Analyzing (22), we observe that although (22) is not a convex optimization problem, it becomes convex when optimizing each variable separately while keeping the others fixed. Therefore, we adopt the AO method to transform the original problem into two sub-problems, which can be solved iteratively. By fixing the power variables, we optimize the beamforming vectors $\mathbf{w}_{c,k,l}$ and $\mathbf{w}_{r,k,l}$, transforming (22) into the beamforming subproblem. We adopt the semidefinite relaxation (SDR) approach by introducing the matrix variables $\mathbf{W}_{c,j,l} = \mathbf{w}_{c,j,l} \mathbf{w}_{c,j,l}^H$ and $\mathbf{W}_{r,j,l} = \mathbf{w}_{r,j,l} \mathbf{w}_{r,j,l}^H$, with the constraints $\mathbf{W}_{c,j,l} \succeq 0$ and $\mathbf{W}_{r,j,l} \succeq 0$.

A. Beamforming Optimization

We formulate the objective function of beamforming subproblem as follows:

$$f(\mathbf{W}_{c,k,l}, \mathbf{W}_{r,k,l}, t_{k,l}) = \sum_{k=1}^K \left(2t_{k,l} \sqrt{P_{r,l}} \sqrt{\text{Tr}(\mathbf{G}_{k,l} \mathbf{W}_{r,k,l} \mathbf{G}_{k,l}^H)} - t_{k,l}^2 \left(P_{k,l} \text{Tr}(\mathbf{G}_{k,l} \mathbf{W}_{c,k,l} \mathbf{G}_{k,l}^H) + \sigma_r^2 \right) \right). \quad (24)$$

Meanwhile, (21f) is also transformed into a convex constraint, which can be expressed in the following form:

$$P_{k,l} \text{Tr}(\mathbf{W}_{c,k,l} \mathbf{h}_{k,l} \mathbf{h}_{k,l}^H) - \gamma_{k,l}^{\text{req}} \left(\sum_{j \neq k} P_{j,l} \text{Tr}(\mathbf{W}_{c,j,l} \mathbf{h}_{k,l} \mathbf{h}_{k,l}^H) + P_{r,l} \sum_{j=1}^K \text{Tr}(\mathbf{W}_{r,j,l} \mathbf{h}_{k,l} \mathbf{h}_{k,l}^H) + \sigma_n^2 \right) \geq 0. \quad (25)$$

Therefore, the corresponding beamforming matrix subproblem is formulated as follows:

$$\max_{\mathbf{W}_{c,j,l}, \mathbf{W}_{r,j,l}, t_{k,l}} f(\mathbf{W}_{c,j,l}, \mathbf{W}_{r,j,l}, t_{k,l}) \quad (26a)$$

$$\text{s.t.} \quad \mathbf{W}_{c,j,l} \succeq 0, \quad \mathbf{W}_{r,j,l} \succeq 0, \quad \forall j \quad (26b)$$

$$(25) \quad (26c)$$

Problem (26) is transformed into a convex optimization problem and can be efficiently solved using a numerical tool.

B. Power Allocation

With the given fixed beamforming matrix $\mathbf{W}_{c,k,l}$ and $\mathbf{W}_{r,k,l}$, the original problem reduces to a subproblem with respect to the power variables. The second sub-objective function is defined as:

$$f(P_{k,l}, P_{r,l}, t_{k,l}) = \sum_{k=1}^K \left(2t_{k,l} \sqrt{P_{r,l}} \sqrt{\text{Tr}(\mathbf{G}_{k,l} \mathbf{W}_{r,k,l} \mathbf{G}_{k,l}^H)} - t_{k,l}^2 \left(P_{k,l} \text{Tr}(\mathbf{G}_{k,l} \mathbf{W}_{c,k,l} \mathbf{G}_{k,l}^H) + \sigma_r^2 \right) \right). \quad (27)$$

Given this objective, the corresponding power allocation subproblem is formulated as follows:

$$\max_{P_{k,l}, P_{r,l}, t_{k,l}} f(P_{k,l}, P_{r,l}, t_{k,l}) \quad (28a)$$

$$\text{s.t.} \quad (21b), (21c), (25). \quad (28b)$$

Algorithm 1 Joint Power and Beamforming Design over Time Slots

Require: $h_{l,k}, G_{l,k}, P_{\max}, \sigma_r^2, \sigma_n^2, \gamma_{k,l}, \forall k, l$
Ensure: $P_{r,l}, P_{k,l}, W_{c,k,l}, W_{r,k,l}, \forall k, l$

- 1: Initialize $l = 1$ and obtain $\{P_{r,0}, P_{k,0}, \mathbf{W}_{c,0}, \mathbf{W}_{r,0}\}$
 - 2: **while** $l \leq L$ and the users remain within AP coverage **do**
 - 3: Conduct EKF steps given by (15)-(17).
 - 4: Gesture decision and communication SINR threshold update, as given by (10) and (7), respectively.
 - 5: Initialize $W_{c,k,l}, W_{r,k,l}$ and $t_{k,l}$.
 - 6: **while** not converged **do**
 - 7: Update $t_{k,l}, \forall k$, by solving Equation (23).
 - 8: Update $W_{c,k,l}, W_{r,k,l}$ by solving Equation (26).
 - 9: Update $t_{k,l}$ by solving Equation (23).
 - 10: Update $P_{k,l}, P_{r,l}$ by solving Equation (28).
 - 11: **end while**
 - 12: Reshape $W_{c,k,l}$ and $W_{r,k,l}$ to obtain rank-one beamforming vectors $w_{c,k,l}$ and $w_{r,k,l}$.
 - 13: $l \leftarrow l + 1$.
 - 14: Perform the EKF update steps given by (18)-(20).
 - 15: **end while**
 - 16: **return** $\{P_{r,l}, P_{k,l}, w_{c,k,l}, w_{r,k,l}\}, \forall k, l$
-

Problem (28) is transformed into a convex optimization problem and can be efficiently solved. Algorithm 1 summarizes the proposed adaptive gesture-aware optimization. The complexity of Algorithm 1 for L timeslot is $\mathcal{O}(L((2KM^2)^{3.5} \log_2(1/\epsilon) + (K+1)^{3.5} \log_2(1/\epsilon)))$, where ϵ is the solution accuracy.

V. SIMULATION RESULTS

We conduct numerical simulations to evaluate the proposed model. Following the setting of $K(f)$ in [13], the simulation parameters are summarized in Table I. The AP is placed at the upper corner of the room. Each gesture action lasts about 1 second. The simulation proceeds in discrete time slots of 0.1 seconds, corresponding to 10 time slots per complete gesture.

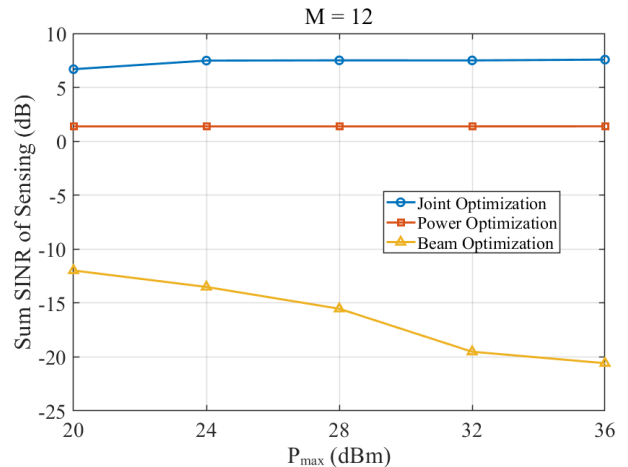
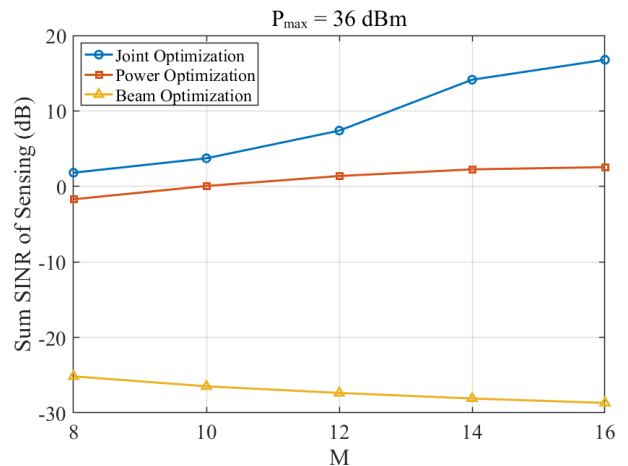
A. Performance under Static Gesture States

We first consider a static scenario with fixed user positions and gesture states, where the communication QoS are available as prior information, and evaluate performance under different antenna numbers and power budgets.

We compare the proposed design with power-only [14] and optimize beam only [15]. As shown in Fig. 2, when the total transmission power constraint increases, both the joint optimization and power-only schemes show slight improvements in sensing performance. This is because, under proportional power initialization and beam-only optimization, the increased communication leakage outweighs the sensing gain. As shown in Fig. 3, the sensing SINR increases with the number of antennas, since a larger array provides higher array gain and finer angular resolution, thereby enhancing the

Table I: Simulation Parameters

Parameter	Value
K : number of users	4
M : number of antennas	12
P_{\max} : maximum Transmit Power	36 dBm
$\text{SINR}_{\text{com}}^{\text{high}}$: high SINR threshold	5
$\text{SINR}_{\text{com}}^{\text{low}}$: low SINR threshold	1
σ_n^2, σ_r^2 : noise power	-90 dBm
T : time slot duration	0.1 s
$K(f)$: absorption coefficient	0.02
h_A : device height when picked up	1.5 m
h_B : device height when put down	1.2 m
ϵ_h : height variation threshold	0.1 m


Figure 2: Sum sensing SINR versus P_{\max}

Figure 3: Sum sensing SINR versus M

reflected sensing signal. By contrast, in the beam-only optimization scheme, the sensing SINR continuously decreases because the sensing power remains fixed and cannot adapt to the increased system resources, while the growing communication power further suppresses the sensing performance.

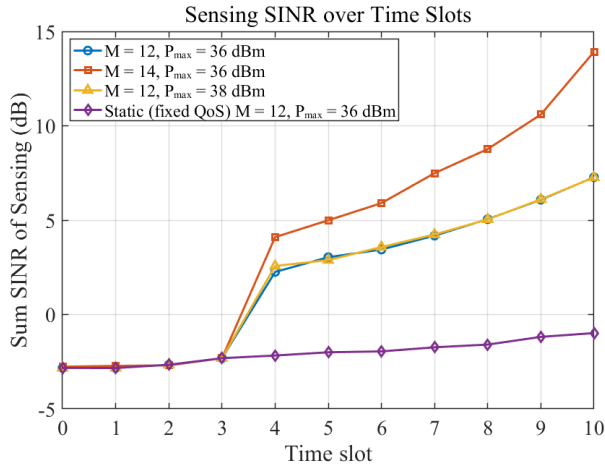


Figure 4: Sum sensing SINR under Dynamic Gesture

B. Performance under Dynamic Gesture Transitions

We next consider a dynamic gesture scenario in which each user’s hand position varies across time slots. At timeslot 0, three users perform the action of putting down the device, while one user performs the action of picking up the device.

We conduct simulations under three different settings to evaluate the impact of antenna number and transmission power on system performance. As shown in Fig 4, the sensing SINR remains low during the first three time slots, since the gesture variation does not exceed the predefined threshold and the system maintains a high communication rate. At time slot 4, the model successfully detects the gesture change and begins to adjust the power allocation and beamforming matrices. Compared with a static baseline without dynamic adaptation, the sum sensing SINR increases significantly and continues to improve in subsequent time slots. These results demonstrate the effectiveness and dynamic adaptability of the proposed model.

VI. CONCLUSION AND FUTURE WORK

This paper investigates a multi-user indoor THz-ISAC system for gesture recognition and proposes a joint optimization algorithm. The system adapts its strategy based on gesture changes, the proposed method improves sensing SINR while maintaining communication performance, and simulation results verify its effectiveness.

The current model assumes fixed user height and stationary users with hand gestures only. In practice, variations in user posture and full-body motion introduce additional complexity. Future work will incorporate intelligent reflecting surfaces (IRS) and tracking mechanisms to improve robustness in dynamic environments.

REFERENCES

- [1] Y. Yang and M. Shikh-Bahaei, “Secure integrated sensing and communication for conventional and isac-dedicated receivers,” in *2023 IEEE 34th Annual International Symposium on Personal, Indoor and Mobile Radio Communications (PIMRC)*, pp. 1–6, 2023.
- [2] W. Shang, Y. Liao, V. Friderikos, and H. Yanikomeroglu, “Unlocking sub-thz by robotic aerial base stations: Joint deployment and wireless backhaul routing,” *IEEE Open Journal of the Communications Society*, 2024.
- [3] L. Li, W. Chen, Z. Chen, T. Hu, W. Mei, and B. Ning, “Enhancing terahertz communications coverage with isac-assisted beam management,” *IEEE Wireless Communications*, vol. 31, no. 1, pp. 34–40, 2024.
- [4] Z. Fang, Y. Lyu, Z. Yu, and C. Han, “Environment reconstruction in terahertz monostatic sensing: Joint millimeter-level geometry mapping and material identification,” *IEEE Journal of Selected Topics in Electromagnetics, Antennas and Propagation*, 2025.
- [5] J. Zhou, Y. Yang, Z. Yang, and M. R. Shikh-Bahaei, “Near-field extremely large-scale star-ris enabled integrated sensing and communications,” *IEEE Transactions on Green Communications and Networking*, vol. 9, no. 1, pp. 404–416, 2024.
- [6] T. Bacchielli, L. Pucci, E. Favarelli, D. Dardari, and A. Giorgetti, “Bistatic thz sensing with mimo-ofdm: A two-stage transmission approach with maximum likelihood estimation,” *Authorea Preprints*.
- [7] V. Towhidlou and M. Shikh-Bahaei, “Adaptive full-duplex communications in cognitive radio networks,” *IEEE Transactions on Vehicular Technology*, vol. 67, no. 9, pp. 8386–8395, 2018.
- [8] Q. Wu, Y. Zhang, Z. Yang, and M. R. Shikh-Bahaei, “Deep channel prediction-based energy-efficient intelligent reflecting surface-aided terahertz communications,” *IEEE Transactions on Wireless Communications*, vol. 23, no. 4, pp. 2946–2960, 2024.
- [9] A. Shafie, N. Yang, S. A. Alvi, C. Han, S. Durrani, and J. M. Jornet, “Spectrum allocation with adaptive sub-band bandwidth for terahertz communication systems,” *IEEE Transactions on Communications*, vol. 70, no. 2, pp. 1407–1422, 2022.
- [10] R. Liu, M. Li, Q. Liu, and A. L. Swindlehurst, “Snr/crb-constrained joint beamforming and reflection designs for ris-isac systems,” *IEEE Transactions on Wireless Communications*, vol. 23, no. 7, pp. 7456–7470, 2023.
- [11] H. Zhang, T. Yang, X. Wu, Z. Guo, and B. Hu, “Robust beamforming design for uav communications based on integrated sensing and communication,” *EURASIP Journal on Wireless Communications and Networking*, vol. 2023, no. 1, p. 88, 2023.
- [12] D. Simon, *Optimal State Estimation: Kalman, H Infinity, and Nonlinear Approaches*. Wiley, 2006.
- [13] Y. Pan, K. Wang, C. Pan, H. Zhu, and J. Wang, “Sum-rate maximization for intelligent reflecting surface assisted terahertz communications,” *IEEE Transactions on Vehicular Technology*, vol. 71, no. 3, pp. 3320–3325, 2022.
- [14] B. Liao, H. Q. Ngo, M. Matthaiou, and P. J. Smith, “Power allocation for massive mimo-isac systems,” *IEEE Transactions on Wireless Communications*, vol. 23, no. 10, pp. 14232–14248, 2024.
- [15] H. Hua, J. Xu, and T. X. Han, “Optimal transmit beamforming for integrated sensing and communication,” *IEEE Transactions on Vehicular Technology*, vol. 72, no. 8, pp. 10588–10603, 2023.